Preprint Title	A switch-based biosensor for the detection and imaging of Hg(II) in vivo by glutathione functionalized gold nanoparticles
Authors	Gufeng Li, Shaoqing Li, Rui Wang, Min Yang, Lizhu Zhang, Yanli Zhang, Wenrong Yang and Hongbin Wang
Publication Date	05 Apr. 2022
Article Type	Full Research Paper
Supporting Information File 1	1Supporting Information File Submitted WHB .pdf; 319.9 KB
ORCID® iDs	Yanli Zhang - https://orcid.org/0000-0002-4119-5233; Wenrong Yang - https://orcid.org/0000-0001-8815-1951

A switch-based biosensor for the detection and imaging of Hg(II) in vivo by glutathione functionalized gold nanoparticles

Gufeng Li,[1] Shaoqing Li,[1] Rui Wang,[1] Min Yang,[1] Lizhu Zhang,[1] Yanli Zhang,[1] Wenrong Yang[*1,2] and Hongbin Wang[*1]

Address:

[1]Key Laboratory of Resource Clean Conversion in Ethnic Regions, School of Chemistry and Environment, Yunnan Minzu University, Kunming 650500, P. R. China, [2]School of Life and Environmental Sciences, Deakin University, Waurn Ponds, Victoria 3216, Australia

Email:

Hongbin Wang[*1] - wanghb2152@126.com

Wenrong Yang[*2] - wenrong.yang@deakin.edu.au

* Corresponding author

Abstract

The optical and biological properties of the tunable functionalized gold nanoparticles (GNPs) tuned have been widely used in the sensing applications. GNPs have a strong binding ability to sulfhydryl groups of thiols. Furthermore, thiols is used as mediators to modify functional molecules to adjust their performance, which can be used to detect metal ions in solution. Herein, we demonstrated the 13 nm GNPs were functionalized by glutathione (GSH) and conjugated by rhodamine 6G derivatives (Rh6G2) which can be used to detect of Hg(II) in cells. The detection of Hg^{2+} is based on the ion-catalyzed hydrolysis reactions of the spiroamide ring of Rh6G2, leading to a significant change in the fluorescence of GNPs-GSH-Rh6G2 from "OFF" to "ON" due to the triggered release. The designed strategy is an effective tool to detect Hg^{2+}. In cytotoxicity experiments, GNPs-GSH-Rh6G2 can penetrate living cells and recognize mercury ions through the fluorescent "ON" form.

Keywords

Introduction

Metal nanoparticles have been widely used in the development and construction of sensor systems and drug carriers due to their excellent biocompatibility, large specific surface area and remarkable photoelectric properties [1]. Among of them, gold nanoparticles (GNPs) have been frequently employed for drug delivery, sensing, imaging and photodynamic therapy owing to their high extinction coefficient, distinct optical properties, excellent biocompatibility, and low toxicity [2–7]. Another advantage of GNPs is that different shapes and sizes are prepared through changing reducing agents and reaction conditions [8]. The surface chemistry of GNPs is modified via ligands with functional groups such as thiol group (-SH), amine ($-NH_2$) and carboxyl (-COOH) [9–11]. The surface of the small GNPs can be easily modified, showing good stability, therefore, they can penetrate the cell membrane, and selectively interact with target biomolecules in cells [12–15].

So far, a variety of functionalized GNPs whose properties are tuned by specific molecules have been reported. For example, Coelho et al. reported that pegylated gold nanoparticles were combined with doxorubicin and varlitinib [16]. The modified pegylated gold nanoparticles exhibited that they can not only reduce the toxicity to normal cells but also improve the inhibitory effect on cancer cells. In another work, Basu et al. designed a novel sensing system using DNA-functionalized Au nanoparticles. AuNPs have a strong binding ability with phosphate and sugar groups in DNA [17]. The combined GNPs-DNA has unique physicochemical properties and was used to detect Mg^{2+}. Furthermore, Liu et al. synthesised a novel probe using gold nanoparticles modified by rhodamine B isothiocyanate and poly (ethylene glycol) (RBITC-PEG-GNPs) [18]. Cytotoxicity assay showed that the cell viability was maintained between 95-100% in the incubation of RBITC-PEG-GNPs with different

concentrations from 0 to 80 nM. Therefore, the strategies to modify or tune GNPs by surface modifications are highly attractive for both environmental monitoring and biological applications.

Surface modification of GNPs by using self-assembled monolayers (SAMs) [19,20], is one of the most attractive strategies to enhance their sensing performance. The surface of GNPs can be modified through the interaction between covalent and non-covalent bonds due to their less steric hindrance [21–23]. The surface of GNPs in some amino acids (containing sulfhydryl), such as cysteine [24–26], 3-mercaptopropionic acid [27] and homocysteine [28], can be modified by Au-S bonds, and they also easily conjugate with drug molecules, and fluorescent dyes [22]. Recently we developed a novel Cu(II)-triggered release system by L-cysteine surface modified gold nanoparticles for molecular delivery and imaging in cells [29]. In this work, well dispersed GNP–L-cysteine was conjugated with Rh6G2 (GNP–L-Cys–Rh6G2) for a molecular release system. By adding Cu(II), we observed switching the GNP–L-Cys–Rh6G2 fluorescence "OFF" to fluorescence "ON" with high stability.

Furthermore, it is worth noting that glutathione (GSH) contains sulfhydryl and amino groups. It can not only conjugate to the nanoparticle surfaces through the thiol group, but also combine with related molecules by its other groups [30]. GSH modified GNPs can improve GNPs' biocompatibility [31–34]. Therefore, GSH can be used to modify the surface of GNPs for improving their stability, safety and biocompatibility of the modified GNPs.

However, in order to enhance the capability of the GSH modified GNPs, additional modification strategy is needed.

In this study, a GSH modified GNPs conjugated rhodamine 6G derivative (GNPs-GSH-Rh6G2) was designed and synthesized in order to effectively tune the properties of GSH functionalized GNPs for sensitive detection of Hg^{2+} and cell imaging. We chose

rhodamine 6G dye because of its excellent light stability, high fluorescence quantum yield and good biocompatibility [35,36]. We observed the functionalized GNPs have excellent selectivity and anti-interference for Hg^{2+}. Furthermore, to evaluate the imaging effects of functionalized GNPs in cells, GNPs-GSH-Rh6G2 was incubated in HeLa cells for CCK-8 Assay. Therefore, we expect that this new triggered release strategy based on the molecular regulation of functionalized GNPs can have potential applications in pollution monitoring, biosensing, and cellular imaging.

Results and Discussion

Synthesis and spectral signature of GNPs-GSH-Rh6G2

As shown in Figure 1a, 13 nm GNPs were synthesized by the protocol reported previously [37], then the surface of GNPs was modified by GSH to form SAMs modified GNPs. Subsequently, carbonyl of Rh6G2 was conjugated with amino group of GSH modified GNPs via Schiff base reaction in a methanol solution [38,39].

It is worth mentioning here that, the pH of the reaction systems played an important role in GSH-Rh6G2. Rh6G2, as an ideal candidate for controlled release molecular system, shows little fluorescence (Figure 1b). In the absence of GNPs, the conjugation of GSH-Rh6G2 shows obvious fluorescence. The S-H group in GSH and the aldehyde group in Rh6G2 undergoes the addition reaction, followed by the formation of unstable intermediates [40]. Ultimately, the carboxylate group (GSH) will give an acidic microenvironment so that a hydrolysis reaction will be occurred, resulting in the formation of RGCOOH (Figure S1, Supporting Information File 1) [41]. The final product of the reaction between Rh6G2 and GSH was proved by TOF-MS analysis (Figure S2, Supporting Information File 1). On the other hand, by adjusting the pH from an unadjusted slightly acidic environment to a neutral environment (pH = 7), a

significant decrease in the fluorescence of GSH-Rh6G2 was observed (Figure S3, Supporting Information File 1). These effects were caused by the pH in the solution system during the reaction.

Consequently, compared with GSH-Rh6G2, the GSH have a high affinity towards GNPs by the sulfhydryl moiety, leading to expose to the amino group. Functional molecules can be directly bound via GSH, providing a stable environment based on the GNPs nanostructure for functional molecules.

The UV-vis absorption and fluorescence spectra of the GNPs-GSH-Rh6G2 were used to evaluate the optical properties of the GNPs-GSH-Rh6G2 as shown in Figure 1c-d. Figure 1c shows the strong absorption peak of 13 nm GNPs with the typical plasmon band of gold nanoparticles at 518 nm. However, the absorption peaks of GNPs-GSH and GNPs-GSH-Rh6G2 were slightly red-shifted from 518 nm to 522 nm and 536 nm, respectively, which are caused by a change in the local dielectric environment and the plasmonic absorption band of GSH and GSH-Rh6G2 modified GNPs [42,43]. The maximum absorption peak of the GNPs-GSH-Rh6G2 is 536 nm, whereas the emission peak is 560 nm (Figure 1d). And then the excitation of GNPs-GSH-Rh6G2 was examined in order to further evaluate its unique emission features. Figure S4 (Supporting Information File 1) shows the emission spectra of GNPs-GSH-Rh6G2 at various excitation wavelengths ranging from 486 to 536 nm. The fluorescence emission wavelength of GNPs-GSH-Rh6G2 appears to exhibit a non-excitation property when the excitation wavelength is changed. Furthermore, the fluorescence intensity of GNPs-GSH-Rh6G2 increased with increasing excitation wavelength, but no complete peak appeared at 526 nm and 536 nm excitation wavelengths. Therefore, the emission intensity of the GNPs-GSH-Rh6G2 at 560 nm under excitation at 516 nm was chosen as the signal of the GNPs-GSH-Rh6G2.
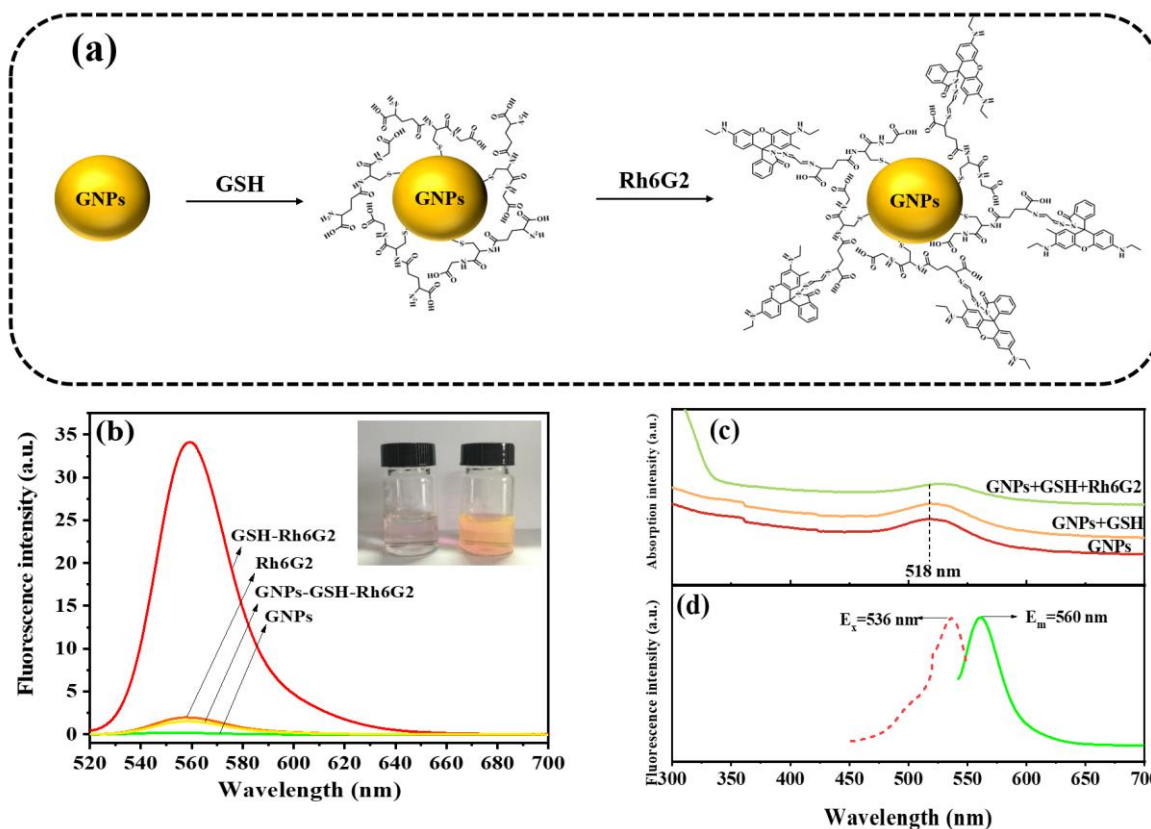
Figure 1: (a) The scheme of functionalized GNPs-GSH-Rh6G2; (b) Fluorescence spectra of GNPs, Rh6G2, GSH-Rh6G2 and GNPs-GSH-Rh6G2 (inset: the left bottle and the right bottle are GNPs-GSH-Rh6G2 and GSH-Rh6G2, respectively); (c) UV-vis spectra of GNPs, GNPs-GSH and GNPs-GSH-Rh6G2; (d) Fluorescence excitation and emission spectra of the GNPs-GSH-Rh6G2.

Characterization of GNPs-GSH-Rh6G2

To confirm the formation of GNPs-GSH-Rh6G2, transmission electron microscopy (TEM) was carried out (inset of Figure 2a-c). As displayed in Figure 2a, the TEM image showed that pure GNPs had well dispersion with a diameter of about 13 nm by DLS measurements. And GSH modified GNPs displays similar morphologies and sizes (Figure 2b) [4,44]. However, while GNPs-GSH were further modified by Rh6G2, as a fluorescent agent, Figure 2c shows the size of the modified GNPs is slightly increased, and no aggregation occurs [45]. Furthermore, the surface charge of GNPs, GNPs-GSH

and GNPs-GSH-Rh6G2 are shown in Figure 2d. Once GNPs were modified with GSH, the surface potential is increased from -34.5 mV to -12.1 mV due to the introduction of positive-charged GSH. After further modifying positive-charged Rh6G2, the zeta potential is increased to -8 mV. These results indicated that the GSH and Rh6G2 were successfully bound with the surface of GNPs.

FTIR spectroscopy of GNPs, GSH, GNPs-GSH and GNPs-GSH-Rh6G2 are presented in Figure 2e. As citrate ions are attached on the surface of GNP, C=O and C-O stretching vibration modes were represented at 1655 cm^{-1} and 1443 cm^{-1}, respectively. The peaks of GSH at 1650 cm^{-1} and 1400 cm^{-1} were found in the IR spectrum of GNPs-GSH, which was attributed to the stretching vibration and asymmetric stretching vibration of COO-. The stretching vibration of S-H disappeared in GNPs-GSH due to the formation of Au-S bonds [46]. These results proved the GNPs-GSH was immobilized on the surface of GNP. Rh6G2 peaks at 1640 cm^{-1} and 1072 cm^{-1} were found on GNPs-GSH-Rh6G2 when Rh6G2 was covalently bound to GNPs-GSH, which was ascribed to the stretching vibration of C=N and C-N. Meanwhile, the peak intensity was also more obviously enhanced than that of GNPs-GSH, indicating that GNPs-GSH-Rh6G2 has been successfully prepared.
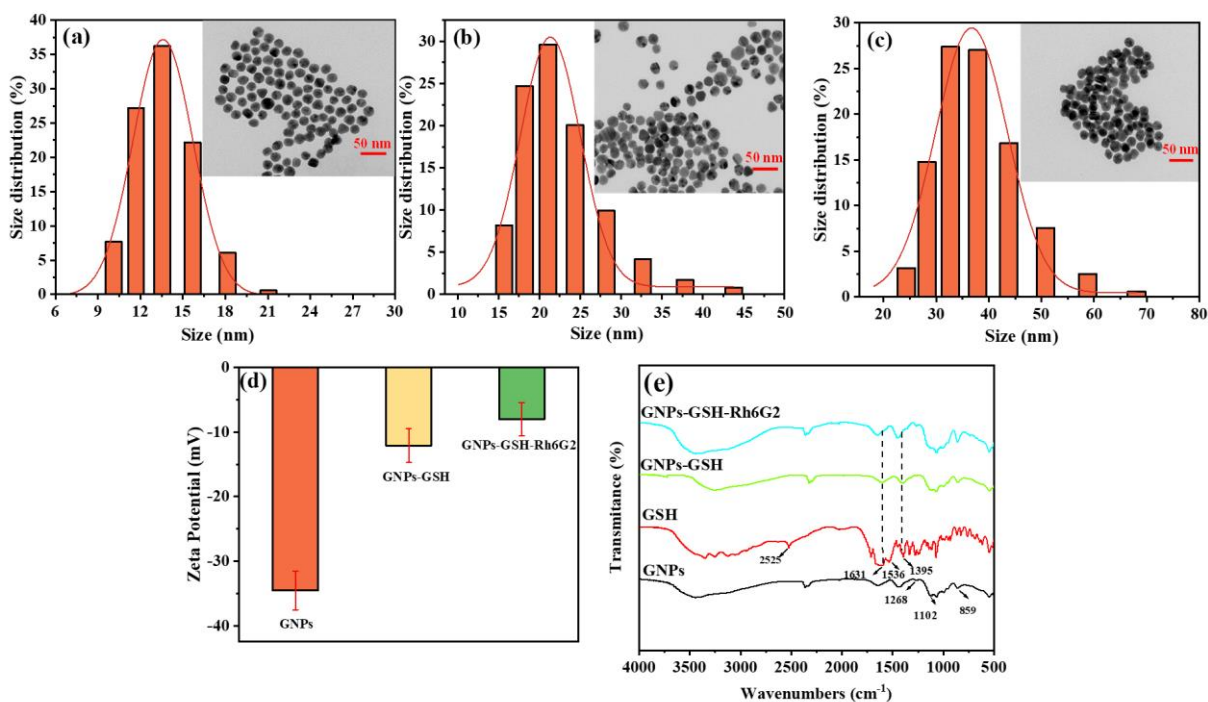
Figure 2: DLS of (a) GNPs, (b) GNPs-GSH and (c) GNPs-GSH-Rh6G2 (inset: the TEM image); (d) Zeta potential of GNPs, GNPs-GSH and GNPs-GSH-Rh6G2; (e) Fourier transforms infrared spectra of GNPs, GSH, GNPs-GSH and GNPs-GSH-Rh6G2.

Synthesis of GNPs-GSH-Rh6G2

In order to fabricate a robust and highly sensitive fluorescent biosensor, we optimized the synthesis conditions of GNPs-GSH-Rh6G2 including the molar ratio of GSH and Rh6G2 and the concentrations of GNPs and GSH. It was reported that the adjacent amino group in the GSH molecule and the aldehyde group in Rh6G2 undergo a cyclization reaction to form a thiazolidine structure through a covalent bond principle [40]. Figure 3a shows that the fluorescence of GNPs-GSH-Rh6G2 reached the maximum when the molar ratio of GSH and Rh6G2 was 1, and the obtained molar ratio is consistent with the theoretical value (the theoretical reaction molar ratio is 1).

To investigate the effect of the concentration of GSH, different amounts of GSH were added. As shown in Figure 3b, when GSH is less than 0.15 µmol, there is basically no fluorescence, which was attributed to the sufficient amount of GSH and Rh6G2 were

9

conjugated on the GNPs surface, because there is no free GSH and Rh6G2 which are capable of reacting with each other. GSH and GNPs are completely conjugated when the amount of GSH was 0.15 µmol. However, we observed excess GSH reacts with Rh6G2 to form a thiazolidine that is easily hydrolyzed to generate fluorescence. Therefore, 0.15 µmol GSH was chosen for the surface modification of GNPs. Figure 3c shows that the fluorescence intensity gradually decreases and tends to be stable with the increase of GNPs. When the amount of GNPs added was more than 0.0726 µmol, the GNPs-GSH-Rh6G2 had little fluorescence, indicating that GNPs and GSH are fully conjugated.

Furthermore, when GSH and Rh6G2 are combined, there will be a strong characteristic absorption peak at 560 nm (Figure S5, Supporting Information File 1). However, when GNPs were introduced into the GHS-Rh6G2, fluorescence disappeared.
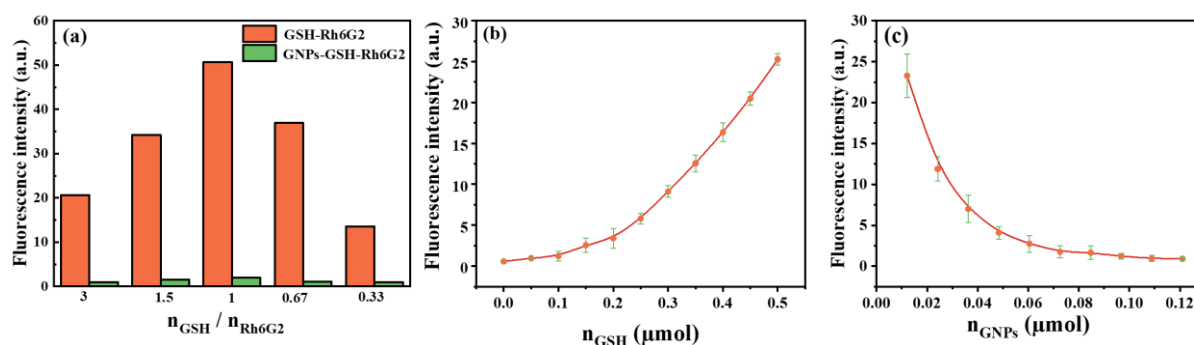

Figure 3: (a) Fluorescence intensity of synthesized GNPs-GSH-RH6G2 at different ratio of n_{GSH} and n_{Rh6G2} (n_{GNPs} is 0.0726 µmol); (b) Fluorescence intensity of GNPs-GSH-Rh6G2 synthesized under different amounts of the substance of GSH (n_{GNPs} and n_{RH6G2} are 0.0726 µmol and 0.15 µmol, respectively); (c) Fluorescence intensity of GNPs-GSH-Rh6G2 synthesized under different amount of GNPs (n_{GSH} and n_{RH6G2} are 0.15 µmol).

We also found the fluorescence of GNPs-GSH-RH6G2 was very weak in the first six hours as shown in Figure 4a, suggesting little fluorescence was observed, as expected. Furthermore, pH is critical in fluorescence intensity. GNPs-GSH-Rh6G2 displays a

larger change in the fluorescence intensity within pH from 1 to 5 (Figure 4b), indicated Rh6G2 tended to be protonated at low pH, which enable ring reactions. However, the fluorescence intensity of the GNPs-GSH-Rh6G2 remained stable in the pH range of 6-11 with a lower fluorescence baseline, which can help the further study in cells and organisms, which as pH 7 is required in biological local environments. The effect of temperature of GNPs-GSH-Rh6G2 was shown in Figure 4c, which shows there is little fluorescent within the temperature range of 25-45 °C. In addition, we also investigated the effect of electrolyte solution (taking NaCl solution as an example) in terms of the stability of GNPs-GSH-Rh6G2. As shown in the Figure 4d, the fluorescence intensity of GNPs-GSH-Rh6G2 remained relatively stable when the concentration of electrolyte solution increased. The GNPs-GSH-Rh6G2 can maintain a lower fluorescence baseline in 0.10 M NaCl solution, which is important for the application in living organisms.
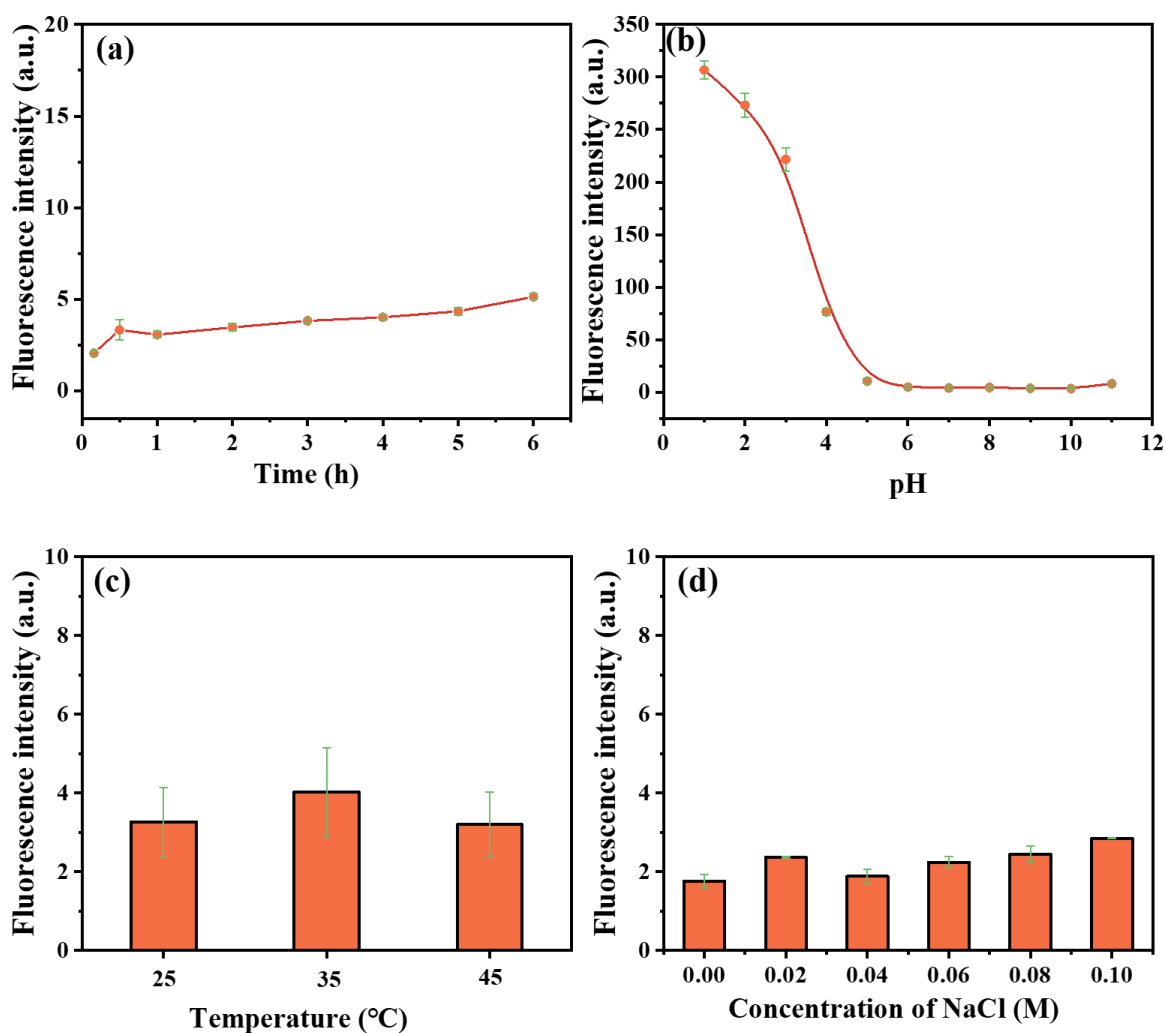
Figure 4: Fluorescence intensity of GNP-GSH-Rh6G2 in HEPES/CH₃OH buffer (1:1 in v/v, 50 mM) under different conditions: (a) Time; (b) pH value; (c) Temperature; (d) The different NaCl concentrations.

Mercury Hg (Ⅱ) detection

We investigated the optical sensing properties of the GNPs-GSH-Rh6G2 by fluorescence spectroscopy. To evaluate the specificity of GNPs-GSH-Rh6G2 for trigger, a variety of cations including Hg^{2+}, Ag^+, K^+, Na^+, Ca^{2+}, Co^{2+}, Cu^{2+}, Fe^{2+}, Mg^{2+}, Mn^{2+}, Pb^{2+}, Zn^{2+}, Al^{3+} and Fe^{3+} were examined. As shown in Figure 5a, except Hg^{2+}, there little optical response. We also studied the effect of GNPs-GSH-Rh6G2 on the fluorescence-triggered release of Hg^{2+} in the presence of other cations (Figure 5b), none of the other ions have a substantial impact on the fluorescence-triggered release.

In addition, Figure 5c-d shows the fluorescence intensity of GNP-GSH-Rh6G2 increased with the increase of Hg^{2+} concentration up to 0.75 mM. We observed the color of GNPs-GSH-RH6G2 is changed from colorless to pink when Hg^{2+} is added (Figure 5e). The fluorescence response showed a good linear relationship in the concentration range of 0.1-0.3 mM. The linear regression equation was $F = 91.51c - 37.05$ ($R^2 = 0.9917$) (c represents Hg^{2+} concentration).
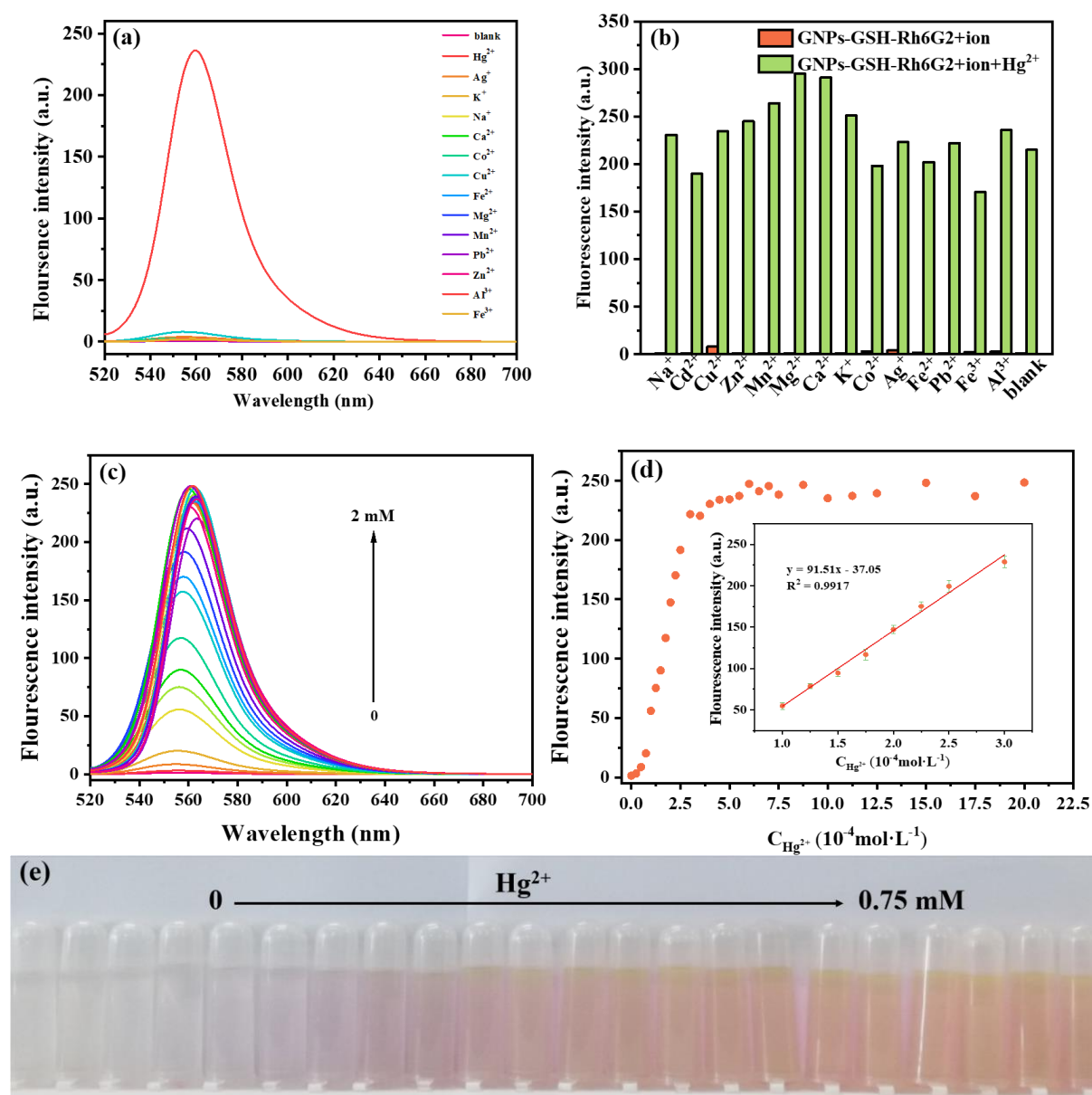

Figure 5: (a) The fluorescence spectra of GNPs-GSH-Rh6G2 with different ions (Hg^{2+}, Na^+, Cu^{2+}, Zn^{2+}, Mn^{2+}, Mg^{2+}, Ca^{2+}, K^+, Co^{2+}, Ag^+, Pb^{2+}, Fe^{3+}, Al^{3+} are 0.75 mM, respectively) in HEPES/CH_3OH buffer (1:1 in v/v, 50 mM, pH = 7); (b) The fluorescence

intensity at 560 nm of GNPs-GSH-Rh6G2 for various metal ions (0.75 mM) in the presence of Hg^{2+} (0.75 mM); (c) The fluorescence spectra of the GNPs-GSH-Rh6G2 in HEPES/CH_3OH buffer (1:1 in v/v, 50 mM, pH = 7) buffer exposed to different concentrations of Hg^{2+}; (d) The fluorescence intensity at 560 nm varied with the concentration of Hg^{2+}; (e) Corresponding photographs of GNPs-GSH-Rh6G2 containing various amount of Hg^{2+}.

GNPs-GSH-Rh6G2 bioimaging in the living cells

To study cell bioimaging of GSH-Rh6G2 and GNPs-GSH-Rh6G2 in living cells, a confocal laser scanning microscopy (CLSM) was performed at different cell incubation times (0-2.5 h). As shown in Figure 6a and 6d, when cultured HeLa cells were incubated with GSH-Rh6G2 and GNPs-GSH-Rh6G2 without Hg^{2+}, there are no obvious intracellular fluorescence signals. After added Hg^{2+} (10 µM) for 1.5 h, the fluorescence in living cells was observed gradually (Figure 6b and 6e), indicated that GSH-Rh6G2 and GNPs-GSH-Rh6G2 could enter the cells and the release of RGCOOH triggered by intracellular Hg^{2+}. Importantly, we found the cellular uptake level of the GNPs-GSH-Rh6G2was higher than that of GSH-Rh6G2. This may be due to the introduction of gold nanostructures, which improves the permeability to cells and make more GNPs-GSH-Rh6G2 enter the cells.

To confirm the effects of different components of the nanostructure in cells, the cytotoxicity of GSH-Rh6G2 and GNPs-GSH-Rh6G2 of different concentrations (0.1, 0.2, 0.3, 0.4 and 0.5 mM) on HeLa cells was evaluated by performing CKK-8 assays. Figure 6g shows an example of this, when cells are incubated with free GSH-Rh6G2 and GNPs-GSH-Rh6G2, HeLa cells viability increases with the increase of time and concentration after 24 h of incubation. In addition, relative to the free GSH-Rh6G2,

14

GNPs-GSH-Rh6G2 demonstrates that gold nanoparticles can improve cell viability, which means that the gold nanosystem possesses high biocompatibility.
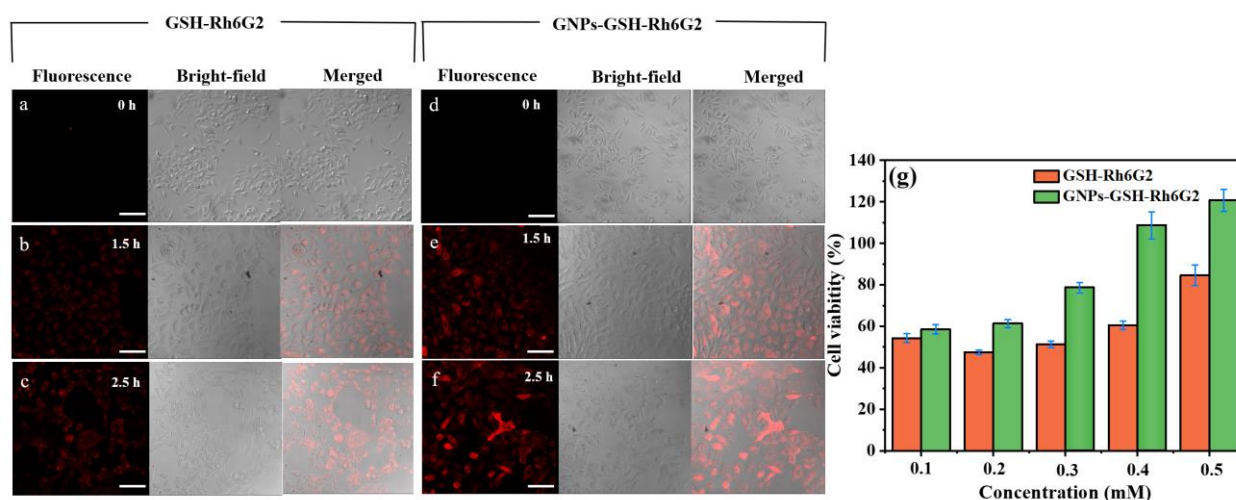

Figure 6: Real-time fluorescence imaging of HeLa cells treated with (a-c) GSH-Rh6G2 and (d-e) GNPs-GSH-Rh6G2 of 100 μL with Hg^{2+} at different incubation times (0, 1.5 and 2.5h). The scale bar is 100 μm. From left to right: images represent fluorescence, bright-field and merge channel fluorescence imaging. (g) Evaluation of cytotoxicity of HeLa cells on various concentrations of GSH-Rh6G2 and GNPs-GSH-Rh6G2 at different concentrations (0.1, 0.2, 0.3, 0.4 and 0.5 mM) for 24 h.

To evaluate the release behavior of GNPs-GSH-Rh6G2, the molecular triggered release started when 30 μL Hg^{2+} was added to the solution. Figure 7 shows that the molecule was released within 20 h, which indicated the sustained molecule-release behavior of the Rh6G2 loaded GNPs-GSH.
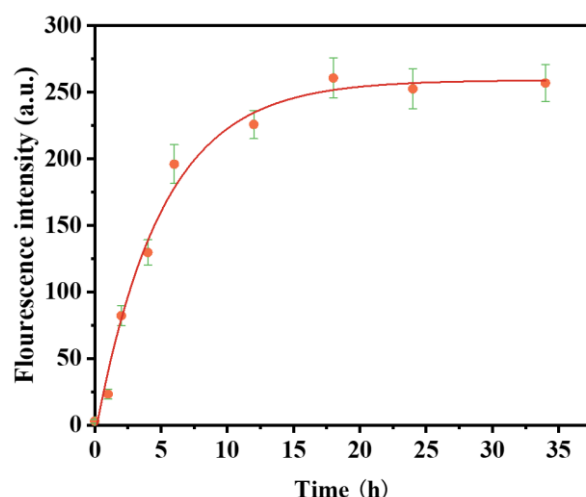
Figure 7: Fluorescence intensity of RGCOOH released from GNPs-GSH-Rh6G2 with Hg^{2+} within 35 h at room temperature in HEPES/CH$_3$OH buffer (1:1 in v/v, 50 mM, pH = 7).

Based on the experimental results, the release mechanism of GNPs-GSH-Rh6G2 by Hg^{2+} was illustrated in Scheme 2a. Rh6G2, when conjugated with GNPs-GSH, did not generate fluorescence owing to the closed spirolactam ring. The protons induce weak fluorescence of lactam spiro-ring framework at acidic pH, which induces the spirolactam ring opening. Therefore, we expected that in the presence of Hg^{2+}, complex formation of Rh6G2-Hg^{2+} leads to ring opening, followed by the release of RGCOOH from the nanoparticle surface via a hydrolysis reaction, and the fluorescence emission is turned on [47].

Furthermore, GNPs-GSH-Rh6G2 did not generate detectable fluorescence signals when it pretreated into the cells. However, when the cells were incubated with both GNPs-GSH-Rh6G2 and Hg^{2+}, red fluorescence images were obtained clearly (Scheme 2b). This is because RGCOOH could be efficiently released from GNPs due to Hg^{2+} promoting ring-opening of the spirocycle group and a hydrolysis reaction occur. Once the RGCOOH molecules were released and diffused into cells, their fluorescence

16

signal was shown "ON". So, by monitoring the fluorescence signal, it is possible to track molecules released to the living cells.
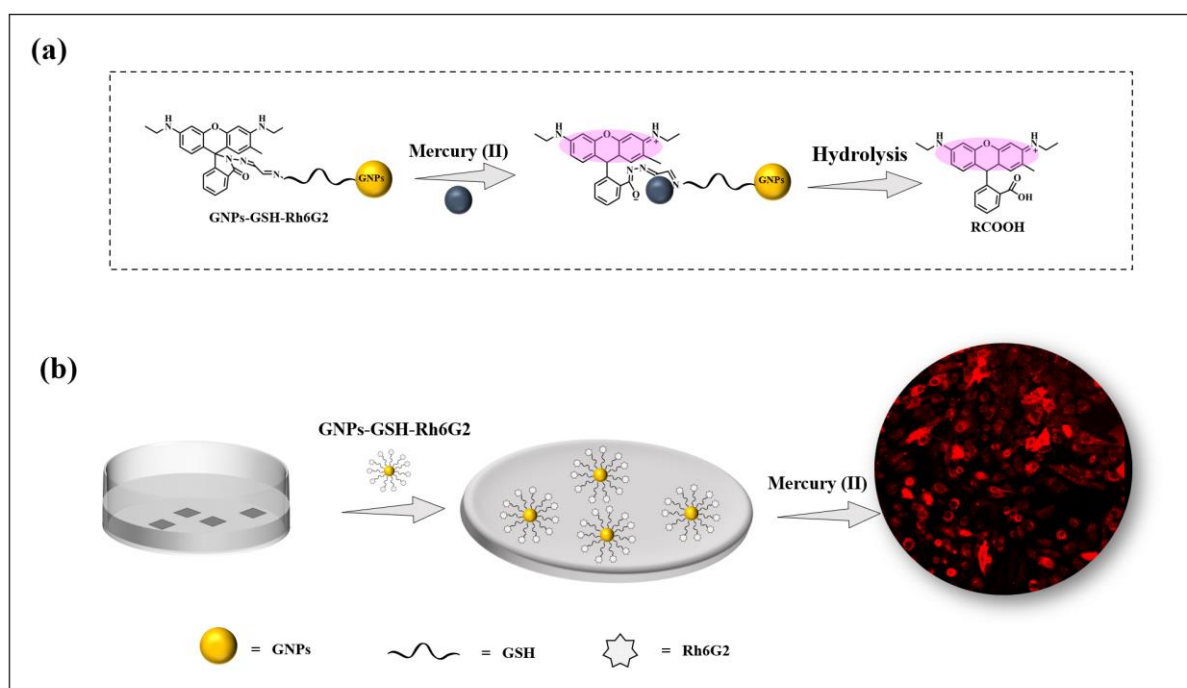
Scheme 2: (a) Schematic illustration of the release mechanism of GNPs-GSH-Rh6G2 to Hg^{2+}; (b) the release of RGCOOH in cells through Hg^{2+}.

Conclusion

In this work, we have demonstrated that GNPs were conjugated with rhodamine 6G derivatives by the surface functionalization of gold nanoparticles with thiol of glutathione, which can be used to simulate the release of fluorescence signal through Hg^{2+}. The fluorescence signal of GNPs-GSH-Rh6G2 in HEPES buffer solution shows a spectral response to the presence of metal ions, which illustrates the sensitivity and selectivity for Hg^{2+}. Further, GSH-Rh6G2 and GNPs-GSH-Rh6G2 were performed in confocal microscopy experiments of Hela cells, which showed that GNPs-GSH-Rh6G2 is more easily internalized into the cell, and then releases RGCOOH. Notably, our strategy was also able to significantly reduce cytotoxicity.

Experimental

Materials and instruments

Gold chloride hydrate (HAuCl$_4$·4H$_2$O) and rhodamine 6G (C$_{18}$H$_{31}$N$_2$O$_3$Cl) were provided from Sinopharm Chemical Reagent Co., Ltd. Trisodium citrate dihydrate and L-Glutathione in the reduced form were purchased from Shanghai Aladdin Bio-Chem Technology Co., Ltd. 4-hydroxyethyl piperazine ethyl sulfonic acid (HEPES) was purchased from Shanghai Mackin Biochemical Co., Ltd. Cervix carcinoma (HeLa cells) were purchased from Kunming Medical University. All reagents are analytical grades (AR).

TEM images were analyzed using a JEM-2100 transmission electron microscope (JEOL, Japan) at an accelerating voltage of 200 kV. UV-vis absorption spectra were obtained using a UV-2100 Spectrophotometer (Shimadzu, Japan). The fluorescence spectra were recorded using an F-7000 Fluorescence spectrophotometer (Hitachi, Japan). The mean particle size and the zeta potential were recorded by using a Zetasizer Nano ZS90 (Malvern, UK). A Nicolet iS10 infrared spectrometer (Nicolet, USA) was used to gather FTIR spectra with a scanning range of 400 cm^{-1} - 4000 cm^{-1}. Fluorescence images of cells were acquired via an OLYMPUS CKX41 inverted fluorescence microscope (Olympus, Japan)/Leica SP5 laser scanning confocal microscope (Leica, Germany). Cell viability was measured by a PectraMax190 microplate reader (Molecular, USA). HPLC-MS was performed on an Agilent-ABQSTAR Pulsar (Agilent, Germany) with a high-resolution mass spectrometer.

Synthesis of GSH-Rh6G and GNPs-GSH-Rh6G2

GNPs with a concentration of about 2.5×10^{-4} M were synthesized using a citrate reduction method [37]. 100 mL of HAuCl$_4$ solution (0.24 mM) was boiled and stirred vigorously. The mixture was swiftly added 3.5 mL of sodium citrate solution (0.34 mM)

until the color changed from yellow to deep red. The mixture was brought to room temperature.

Compound Rh6G2 has been synthesized in previous study [40] and its chemical structure was confirmed. The GSH and Rh6G2 functionalized GNPs were prepared as follows: Firstly, 150 µL of GSH stock solution (1 mM) prepared in deionized water was added into 300 µL of 13 nm GNPs solution for 0.5 h. Then, 2 mL Rh6G2 stock solution (75 µM) were added to reaction mixtures at room temperature for 2 h to acquire GNPs-GSH-Rh6G2. GSH-Rh6G2 were prepared by a similar process, in which 150 µL of GSH stock solution (1 mM) was added into 2 mL Rh6G2 stock solution (75 µM), which was adjusted to pH = 7 with NaOH (1 M). Nitrogen was used to protect the reaction for 2 h to acquire GSH-Rh6G2.

Fluorescence measurements

The fluorescence emission intensity was measured at 560 nm with an excitation wavelength of 516 nm and the excitation and emission slits set were at 2.5 nm. 2.45 mL of GNPs-GSH-Rh6G2 was diluted to 4.00 mL by HEPES/CH_3OH buffer solution (1:1 in v/v, 50 mM, pH = 7), respectively. The solution of GNPs-GSH-Rh6G2 with metal ions was prepared by adding 30 µL stock solution of Hg^{2+}, Ag^+, K^+, Na^+, Ca^{2+}, Co^{2+}, Cu^{2+}, Fe^{2+}, Mg^{2+}, Mn^{2+}, Pb^{2+}, Zn^{2+}, Al^{3+} and Fe^{3+} (0.75 mM). Each solution of GNPs-GSH-Rh6G2/ion was prepared in spectral cuvettes that were carefully cleaned to avoid contamination. Fluorescence spectra were measured after mixing well to fully interact with the GNPs-GSH-RH6G2. To reduce experimental mistakes, all tests were done in triplicate.

Cell culture and imaging of intracellular molecular release

HeLa cells were incubated in Dulbecco's modified Eagle medium Dulbecco (DMEM) (the density is about $2x10^4$ cells per well) at 37 °C in a 5% CO_2 for 48 h. After adding 100 µL of GSH-Rh6G2 and GNPs-GSH-Rh6G2 for 1 h, HEPES buffer was washed

three times. And then 30 μL Hg (II) was added for a different time. Residual ions were washed with HEPES buffer before imaging. Confocal laser scanning microscopy with a 543 nm excitation was used to collect the fluorescence.

Cytotoxicity assays

Cytotoxicity assays were used to investigate the bio-safety of GSH-Rh6G2 and GNPs-GSH-Rh6G2. HeLa cells with 8 x 10^3 per well were incubated in a 96-well plate overnight. 100 μL of GSH-Rh6G2 and GNPs-GSH-Rh6G2 at different concentrations were added in DMEM medium at 37 °C in a 5% CO_2 for 24 h. The medium was replaced by a 110 μL mixture (100 μL of EMEM medium completed with 10% fetal bovine serum (FBS) and 10 μL Cell Counting Kit-8 reagent (CCK-8)), and incubated for 2 h. Then, it was washed with HEPES buffer. A microplate reader was used to measure the absorbance at 450 nm. Each group had six parallel wells, and the experiment was repeated three times. The cells were calculated according to this equation: cell viability (%) = [A_{450} (sample) - A_{450} (blank)] / [A_{450} (control) - A_{450} (blank)] x 100%.

Supporting Information

Supporting Information File 1: Additional experimental data.

Acknowledgements

Funding

References

1.   Zhang, Q.; Gong, Y.; Guo, X.; Zhang, P.; Ding, C. *ACS Appl Mater Inter.* **2018**, *10* (41), 34840–34848. doi:10.1021/acsami.8b12897

2.   Thambiraj, S.; Hema, S.; Ravi Shankaran, D. *Mater Today: Proceedings.* **2018**, *5* (8, Part 3), 16763–16773. doi:10.1016/j.matpr.2018.06.030

3.   Hou, Z.; Wang, Z.; Liu, R.; Li, H.; Zhang, Z.; Su, T.; Yang, J.; Liu, H. *J Nanobiotechnol.* **2019**, *17* (1), 88. doi:10.1186/s12951-019-0522-y

4.   Xu, J.; Yu, H.; Hu, Y.; Chen, M.; Shao, S. *Biosens Bioelectron.* **2016**, *75*, 1–7. doi:10.1016/j.bios.2015.08.007

5.   Lou, X.; Zhang, Y.; Qin, J.; Li, Z. *Chem-Eur J.* **2011**, *17* (35), 9691–9696. doi:10.1002/chem.201100389

6.   Liu, M.; Li, Q.; Liang, L.; Li, J.; Wang, K.; Li, J.; Lv, M.; Chen, N.; Song, H.; Lee, J.; Shi, J.; Wang, L.; Lal, R.; Fan, C. *Nat Commun.* **2017**, *8* (1), 15646. doi:10.1038/ncomms15646

7.   Penon, O.; Marín, M. J.; Russell, D. A.; Pérez-García, L. *J Colloid Interf Sci.* **2017**, *496*, 100–110. doi:10.1016/j.jcis.2017.02.006

8.   Carnovale, C.; Bryant, G.; Shukla, R.; Bansal, V. *Prog Mater Sci.* **2016**, *83*, 152–190. doi:10.1016/j.pmatsci.2016.04.003

9.   Rana, S.; Bajaj, A.; Mout, R.; Rotello, V. M. *Adv Drug Deliver Rev.* **2012**, *64* (2), 200–216. doi:10.1016/j.addr.2011.08.006

10.   Vigderman, L.; Zubarev, E. R. Adv Drug Deliver Rev. **2013**, *65* (5), 663–676. doi:10.1016/j.addr.2012.05.004

11.   Sener, G.; Uzun, L.; Denizli, A. *Anal. Chem.* **2014**, *86* (1), 514–520. doi:10.1021/ac403447a

12.   Hinton, T. M.; Grusche, F.; Acharya, D.; Shukla, R.; Bansal, V.; Waddington, L. J.; Monaghan, P.; Muir, B. W. *Toxicol Res-UK.* **2014**, *3* (1), 11–22. doi:10.1039/C3TX50075F

13.   Ning, Z.; Cheung, C. S.; Fu, J.; Liu, M. A.; Schnell, M. A. *Sci Total Environ.* **2006**, *367* (2–3), 822–830. doi:10.1016/j.scitotenv.2006.02.017

14.   Guo, Y.; Zhang, Y.; Shao, H.; Wang, Z.; Wang, X.; Jiang, X. *Anal Chem.* **2014**, *86* (17), 8530–8534

15.   Chithrani, B. D.; Ghazani, A. A.; Chan, W. C. *Nano letters.* **2006**, *6* (4), 662–668. doi:10.1021/nl052396o

16.   Coelho, S. C.; Reis, D. P.; Pereira, M. C.; Coelho, M. A. N. *Pharmaceutics.* **2019**, *11* (11), 551. doi:10.3390/pharmaceutics11110551

17.   Basu, T.; Rana, K.; Das, N.; Pal, B. *Beilstein J. Nanotechnol.* **2017**, *8*, 762–771. doi:10/gn28dt

18.   Liu, D.; Wang, S.; Swierczewska, M.; Huang, X.; Bhirde, A. A.; Sun, J.; Wang, Z.; Yang, M.; Jiang, X.; Chen, X. *ACS Nano* **2012**, *6* (12), 10999–11008. doi:10/f4gg3x

19.   Gooding, J. J.; Mearns, F.; Yang, W.; Liu, J. Electroanal. **2003**, *15* (2), 81–96. doi:10/c5s97w

20.   Gooding, J.; Yang, W. *L' Actualite Chimique.* **2008**, *320* (321), 85–89.

21.   Yuan, H.; Ji, W.; Chu, S.; Liu, Q.; Qian, S.; Guang, J.; Wang, J.; Han, X.; Masson, J.-F.; Peng, W. *ACS Sens.* **2019**, *4* (3), 704–710. doi:10.1021/acssensors.8b01558

22.   Chen, Y.; Xianyu, Y.; Jiang, X. *Accounts Chem Res.* **2017**, *50* (2), 310–319. doi:10.1021/acs.accounts.6b00506

23.   Yu, C.-J.; Tseng, W.-L. *Langmuir.* **2008**, *24* (21), 12717–12722. doi:10.1021/la802105b

24.   Yang, W.; Gooding, J. J.; He, Z.; Li, Q.; Chen, G. *J Nanosci Nanotechno.* **2007**, *7* (2), 712–716. doi:10/gpmpqs

25.   Zhang, Y.; Liu, J.; Li, D.; Dai, X.; Yan, F.; Conlan, X. A.; Zhou, R.; Barrow, C. J.; He, J.; Wang, X.; Yang, W. *ACS Nano.* **2016**, *10* (5), 5096–5103. doi:10.1021/acsnano.6b00216

26.   Zhang, Y.; Kong, N.; Zhang, Y.; Yang, W.; Yan, F. *Theranostics.* **2017**, *7* (5), 1214–1224. doi:10/f94t9c

27.   Chang, H.-Y.; Hsiung, T.-M.; Huang, Y.-F.; Huang, C.-C. *Environ. Sci. Technol.* **2011**, *45* (4), 1534–1539. doi:10.1021/es103369d

28.   Huang, C.-C.; Chang, H.-T. *Anal. Chem.* **2006**, *78* (24), 8332–8338. doi:10.1021/ac061487i

29.   Li, S.; Huang, W.; Tan, W.; Zhang, L.; Zhang, Y.; Shi, H.; Mathesh, M.; Barrow, C. J.; Yang, W.; Wang, H. *Mol. Syst. Des. Eng.* **2021**, 6, 825–831. doi:10.1039/D1ME00074H

30.   Chu, W.; Zhang, Y.; Li, D.; Barrow, C. J.; Wang, H.; Yang, W. *Biosens Bioelectron.* **2015**, *67*, 621–624. doi:10.1016/j.bios.2014.09.077

31.   Steckiewicz, K. P.; Barcinska, E.; Sobczak, K.; Tomczyk, E.; Wojcik, M.; Inkielewicz-Stepniak, I. *Int J Med Sci.* **2020**, *17* (6), 824–833. doi:10.7150/ijms.40827

32.   Pem, B.; Pongrac, I. M.; Ulm, L.; Pavičić, I.; Vrček, V.; Jurašin, D. D.; Ljubojević, M.; Krivohlavek, A.; Vrček, I. V. *Beilstein J. Nanotechnol.* **2019**, *10* (1), 1802–1817. doi:10.3762/bjnano.10.175

33.   Chakrabarty, S.; Maity, S.; Yazhini, D.; Ghosh, A. *Langmuir.* **2020**, acs.langmuir.0c01527. doi:10.1021/acs.langmuir.0c01527

34.   Pem, B.; Pongrac, I. M.; Ulm, L.; Pavičić, I.; Vrček, V.; Domazet Jurašin, D.; Ljubojević, M.; Krivohlavek, A.; Vinković Vrček, I. *Beilstein J. Nanotechnol.* **2019**, *10*, 1802–1817. doi:10/gn4596

35.   Beija, M.; Afonso, C. A.; Martinho, J. M. *Chem Soc Rev.* **2009**, *38* (8), 2410–2433. doi:10.1039/b901612k

36.   Magde, D.; Wong, R.; Seybold, P. G. *Photochem Photobiol.* **2007**, *75* (4), 327–334. doi:10.1562/0031-8655(2002)0750327FQYATR2.0.CO2

37.   Weng, Z.; Wang, H.; Vongsvivut, J.; Li, R.; Glushenkov, A. M.; He, J.; Chen, Y.; Barrow, C. J.; Yang, W. Anal Chim Acta. **2013**, *803*, 128–134. doi:10/f5gj5z

38.   Jiao, Y.; Liu, X.; Zhou, L.; He, H.; Zhou, P.; Duan, C. *Sensor Actuat B-Chem.* **2017**, *247*, 950–956. doi:10.1016/j.snb.2017.01.124

39.   Guo, P.; Liu, L.; Shi, Q.; Yin, C.; Shi, X. *J Mol Struct.* **2017**, *1130*, 150–155. doi:10.1016/j.molstruc.2016.10.027

40.   Li, H.; Fan, J.; Wang, J.; Tian, M.; Du, J.; Sun, S.; Sun, P.; Peng, X. *Chem. Commun.* **2009**, No. 39, 5904-5906. doi:10.1039/b907511a

41.   Ou-Yang, J.; Li, C.-Y.; Li, Y.-F.; Fei, J.; Xu, F.; Li, S.-J.; Nie, S.-X. *Sensor Actuat B-Chem.* **2017**, *240*, 1165–1173. doi:10.1016/j.snb.2016.09.074

42.   Barzan, M.; Hajiesmaeilbaigi, F. *Eur. Phys. J. D.* **2016**, *70* (5), 121. doi:10.1140/epjd/e2016-70088-6

43.   Heo, D. N.; Yang, D. H.; Moon, H.-J.; Lee, J. B.; Bae, M. S.; Lee, S. C.; Lee, W. J.; Sun, I.-C.; Kwon, I. K. *Biomaterials.* **2012**, *33* (3), 856–866. doi:10.1016/j.biomaterials.2011.09.064

44.   Yang, Y.; Lu, L.; Tian, X.; Li, Y.; Yang, C.; Nie, Y.; Zhou, Z. *Sensor Actuat B-Chem.* **2019**, *278*, 82–87. doi:10.1016/j.snb.2018.09.072

45.   Narode, Y. M.; Mokashi, V. M.; Sharma, G. K. *J Lumin.* **2018**, *201*, 479–484. doi:10.1016/j.jlumin.2018.05.011

46.   Aryal, S.; B.K.C., R.; Dharmaraj, N.; Bhattarai, N.; Kim, C. H.; Kim, H. Y. *Spectrochim Acta A.* **2006**, *63* (1), 160–163. doi:10/fbxzvn

47.   Du, J.; Fan, J.; Peng, X.; Sun, P.; Wang, J.; Li, H.; Sun, S. *Org Lett.* **2010**, *12* (3), 476–479. doi:10.1021/ol902590g